# Experimental, numerical, and theoretical analysis of taper belleville spring

Journal Title
XX(X):1–12

DOI: 10.1177/ToBeAssigned
www.sagepub.com/
SAGE

Umesh Singh[1], Manish Trikha[2], K.R.Y Simha[3]and Ashitava Ghosal[3]

Abstract
Uniform thickness belleville springs(UBS) are a suitable replacement for coil springs in many applications due to their ability to take higher loads and their relatively small and compact size. This paper presents an experimental, numerical and theoretical analysis of the taper belleville spring(TBS). Experimental results on a normal taper belleville spring (NTBS), fabricated from stainless steel alloy (SS304), are presented. Non linear elastic-plastic finite element simulations support the experimental behaviour reasonably well. A correction factor based on Timoshenko's theory of plates, to match the finite element analysis(FEA) results for NTBS, is presented. Reverse taper belleville spring (RTBS) analysis shows that it can store more elastic strain energy than UBS and NTBS. An optimisation study on TBS geometrical parameters is performed to attain maximum energy absorption for the null stiffness region.

Keywords
Non-linear load–deflection, Null stiffness, Tapered belleville spring, Analytical formulation, Energy density, Correction factor, Experiments

## Introduction

Uniform thickness belleville springs (UBS), also commonly called disc springs, are frequently used automotive components such as transmission in passenger vehicles and in the braking systems for off-highway equipment (1; 2). UBS stacked in series or parallel arrangements are also suitable for vibration isolation during shock loading (3; 4).

Almen & Laszlo (5) were the pioneers in the study of non-linear UBS behavior and presented results with various height and thickness combinations. Exploiting non-linear behaviour, UBS can be used as a positive, negative, and null stiffness spring. The null stiffness of the UBS spring makes it useful in situations where sudden load transfer is restricted. Kobelev (6) presented a closed-form solution for forces and stresses in an UBS using the variation method. Du et al. (7) derived a new analytical formula concerning geometric and material parameters to characterize the non-linear load versus deflection properties using the Galerkin method. There have been also extensive studies on non-uniform belleville springs – Rosa et al. (8) analyzed a TBS with linearly varying thickness and obtained its load versus deflection characteristics. It was shown that the null stiffness region is improved compared to the UBS (5) and there were constant stress state conditions on both the spring surfaces thereby making it favourable for fluctuating loads. Saini et al. (9) studied the parabolically varying thickness belleville spring and showed further improvement in the span of the null slope zone in the stiffness curve compared to a TBS (8). Fawazi et al. (10) derived an improved equation for a coned slotted disc spring with a lever arm, developed the load versus deflection equation using the energy method and the result was compared with a straight slotted disc spring. Pederson et al. (11) studied the stiffness and stress distribution of the uniform as well as the variable thickness belleville spring using the non-linear three-dimensional finite element analysis. Dubey et al. (12) numerically analyzed the behaviour of the stresses on the inner and outer surface of the spring with the variation of outer and inner diameter ratio and height to thickness ratio. Ramhormozian et al. (13) demonstrated the use of slotted UBS, within the elastic region of the bolt, used for the retention of the beam to a column using a sliding hinge joint bolt under tension. Venkatesh et al. (14) analyzed the stresses for different types of UBS – inside slotted, outside slotted, and holes with slotted UBS and proposed the best UBS according to their uses. Zhu et al. (15) studied the negative stiffness region of the grooved disk spring with numerical analysis and presented experimental data. Chaturvedi et al. (16) explored the mechanical behaviour of stepped section disk springs and an analytical derivation for the load as a function of deflection is presented. Leininger et al. (17) proposed a new formula, based on four edge radii and two angles of the inner and outer faces, and presented finite element simulations of disk springs with

[1]U.R.Rao Satellite Centre, Bangalore, Karnataka, India
[2]Human Space Flight Centre, Bangalore, Karnataka, India
[3]Indian Institute of Science, Bangalore, Karnataka, India

Corresponding author:
Ashitava Ghosal, Department of Mechanical Engineering, Indian Institute of Science, Bangalore, Karnataka, India.
Email: asitava@iisc.ac.in

rounded edges and a non-rectangular cross-section to model the fillet at the edges in the manufactured disk spring. Ferrari et al. (18) presented an approach to determine the load-deflection plot for disk springs with contact flats and reduced thickness. The contact flats are shown to improve the definition of the point where the load is applied. Moreover, particularly for spring stacks, it reduces the friction at the guide rod of the stacking. Optimisation tools have been developed for designers to select UBS geometry and the arrangements of belleville springs to obtain a desired load-deflection characteristics (19).

In addition to the load-displacement characteristics, the friction in a belleville spring, especially in a stack, plays an important part in their usage and several researchers have studied the friction aspect of a belleville spring. Maharjan et al. (20) explored the area of frictional loss during spring loading and its effect on the stiffness curve. This is done by calculating the displacement of different points of UBS during the event of loading and unloading using a linear interpolation method and experiments were conducted to support the analytical derivation. Xiao et al. (21) developed a non-linear regression method to obtain the friction and torque relationship for UBS with friction material. Mastricola et al. (22) discuss the effect of the asymmetric friction condition of edges on the stiffness curve of a coned disk spring with square edges. Although there is a significant amount of literature on belleville springs, there is a need for extending theoretical, numerical, and experimental analysis for optimizing taper configurations. Comparing RTBS with NTBS is essential to validate the conclusion drawn by Rosa et al. (8). In particular, the energy storage capability of RTBS vis-a-vis NTBS can become a crucial factor in designing compact stacked TBS systems. Frictional contact plays another unpredictable role in the overall design and analysis and can be assessed only through experiments. Finally, plasticity and hysteresis play a significant role in spring design, and belleville spring is no exception to this general concern. The research objective of this work is to design a small-sized tapered belleville spring for the null stiffness region to absorb low velocity impact energy. The research objective is also to examine the assumptions and approximations used in existing theoretical formulations. Finally, in this work, we compare the energy absorption in normal and reverse tapered belleville springs.

Several SS304 NTBS were fabricated. Experiments conducted on a Universal Testing Machine (UTM) to find the load versus deflection characteristics showed elastic-plastic deformation. Extensive elastic-plastic finite element simulations with the same geometry and in the same range of deformation as in experiments were performed in ABAQUS (23). These simulations showed a good match with NTBS experimental results. Next, an analytical formulation that includes the null stiffness region and Poisson's ratio is presented and FEA were performed on UBS, NTBS and RTBS geometries. It was observed that there were differences in the results obtained from FEA and analytical results which were significant in the case of NTBS. A stiffness correction factor, based on the theory of plates and shells by Timoshenko & Krieger (24) is proposed and it is shown that the use of this correction factor results in a much closer match with the FEA for a NTBS. It is also demonstrated that the FEA match reasonably well for UBS and RTBS geometry even without the use of the correction factor. Simulations also show that RTBS stores more energy density than UBS or NTBS. Thus, RTBS is desirable when more energy needs to be processed.

This paper attempts to consolidate experimental, numerical, and analytical results on TBS configurations to gain an overall appreciation of the two main non-linearities: elastic and plastic. This paper is organized as follows: In the next section, we present NTBS experiments performed and the results obtained. this is followed by elastic-plastic FEA on NTBS for comparison with theory and experiment. In the theoretical formulation for NTBS, we include Poisson's ratio also unlike Rosa et.al(8). The section on the correction factor improves upon the results derived by Almen and Lazlo (5) and Rosa et al. (8) and the use of the correction factor is shown to give a better comparison with FEA for NTBS. Finally, the energy storage capability of RTBS vis-a-vis NTBS is discussed before presenting some experimental results on the cyclic loading of SS304 NTBS. Conclusions drawn from this investigation constitute the last section.

## Experiments with TBS

Fig. 1 shows a 3D and section view of a NTBS. The NTBS geometry is determined by the outer radius $a$, inner radius $b$, thickness at radii $a$ and $b$ denoted by $t_a$ and $t_b$ respectively, the height difference $h$ between the two faces at 'a' and 'b' and the angle $\beta$ as shown in Fig. 1b. The NTBS material parameters and properties are given in Table1.

Table 1. Material and geometric parameter of NTBS

| Sl no | Fabricated spring specification | |
|---|---|---|
| 1 | Material | SS304 |
| 2 | $a$ | 25 mm |
| 3 | $b$ | 12.5 mm |
| 4 | $t_a$ | 3 mm |
| 5 | $t_b$ | 1.5 mm |
| 6 | $h$ | 2.7 mm |
| 7 | $\beta$ | 12.18° |
| 8 | Hardness | 34 HRC |
| 9 | E | 195 GPa |
| 10 | Density | 7.8 gm/cm$^3$ |
| 11 | Poisson's ratio ($\nu$) | 0.27 |
| 12 | Yield Stress of SS304 | 205 MPa |

Loading experiments were conducted on a UTM with a maximum capacity of 100 kN as shown in Fig. 3. A digital vertical scale was used for vertical displacement. The maximum time of loading and unloading was set for 10 min, respectively and a load cut-off at 90% of UTM capacity was set for a successful experiment and

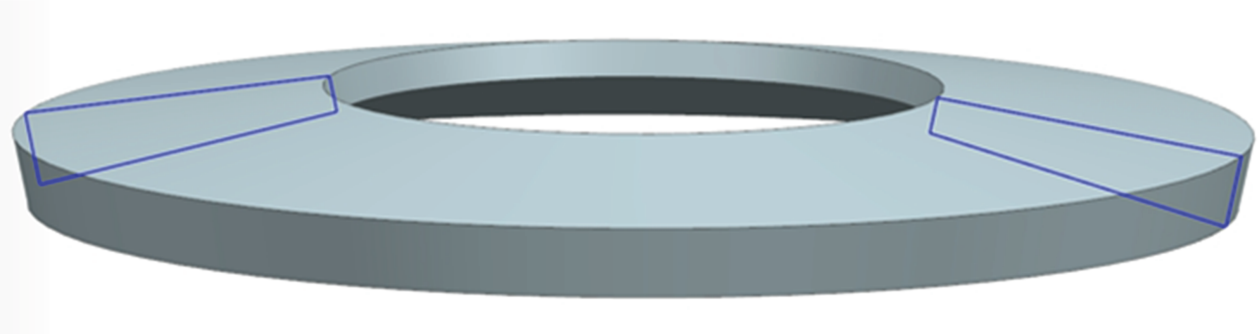

(a) 3D view of a TBS

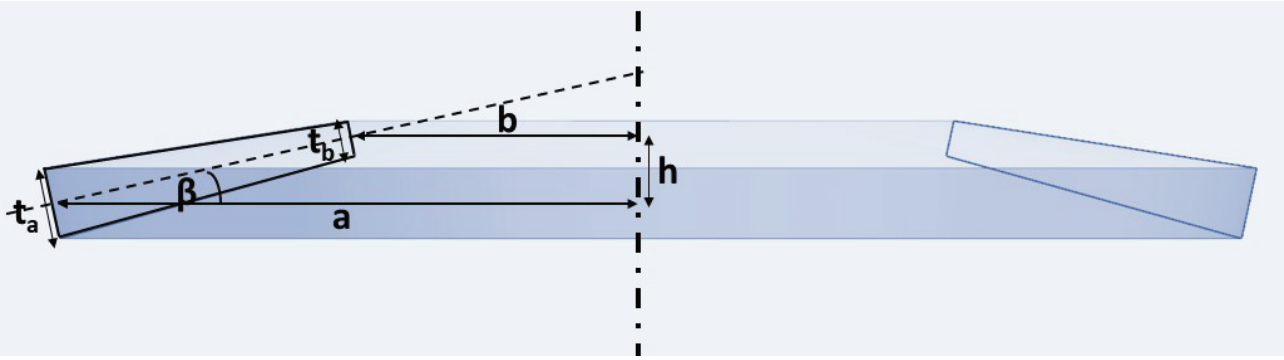


(b) Geometric parameters of a TBS

Figure 1. Schematic of a TBS

Figure 2. Fabricated disc spring

to secure the load cell. During the tests, it was ensured that the spring axis coincided with the center of the axis of the fixture. A loading rate of 0.2 mm/min was used. Three experiments were done for loading till the deflection $\delta$ was the same as height $h$. To understand the hysteresis behavior of the spring, experiments were done for cyclic loading on the spring with displacements of 0 0.5 mm – 0, 0 – 0.75 mm – 0, 0 – 1 mm – 0, 0 1.5 mm – 0, 0 1.75 mm – 0, and 0 2 mm – 0. Details of the cyclic loading tests are provided in a later section.

The main results of NTBS experiments:

- NTBS exhibited non-linear behavior with the increased flat region in the deflection range (see Fig. 4). Multiple experiments show similar behaviour on the stiffness curve with a small scatter, caused by fabrication variation.
- The spring is fabricated with $h/t_c < \sqrt{2}$ where in the null stiffness is not expected according to NTBS theory (8). Thus the flat region observed is due to plastic deformation.
- The fabricated NTBS material has a low yield strength of about 205 MPa and the spring angle ($\approx 12°$) results in plastic deformation due to high stress build-up in the section.
- From the data of the three experiments, it can be seen that the load vs deflection characteristics of the fabricated spring are reasonably repeatable. The maximum variation of 500 N observed at 0.5 mm deflection signals the onset of the plasticity.

To better understand the experimental behavior of an NTBS, numerical analysis is discussed in the next section.

## FEA and simulation

This section outlines the FEA conducted in this study, focusing on predicting the deformation behavior of SS304 NTBS under axial loading using Abaqus (23). Fig. 5a depicts the axisymmetric FE model, highlighting its geometric dimensions and applied boundary conditions. The NTBS is discretized utilizing

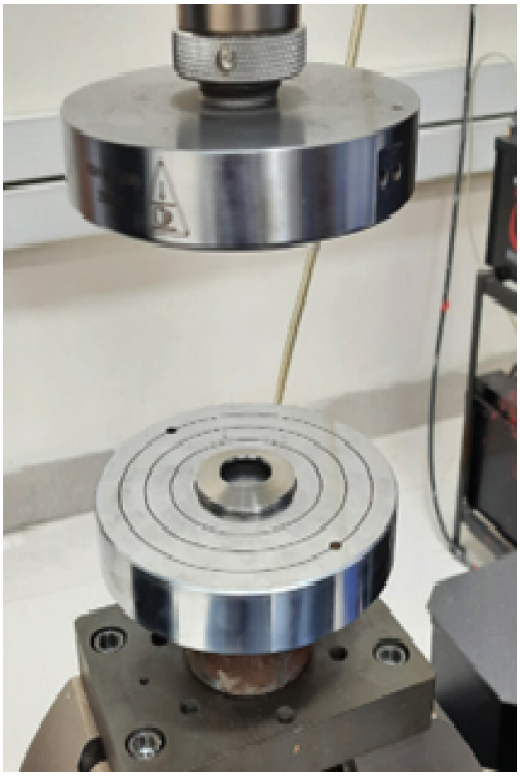

(a) Disc spring on UTM from top

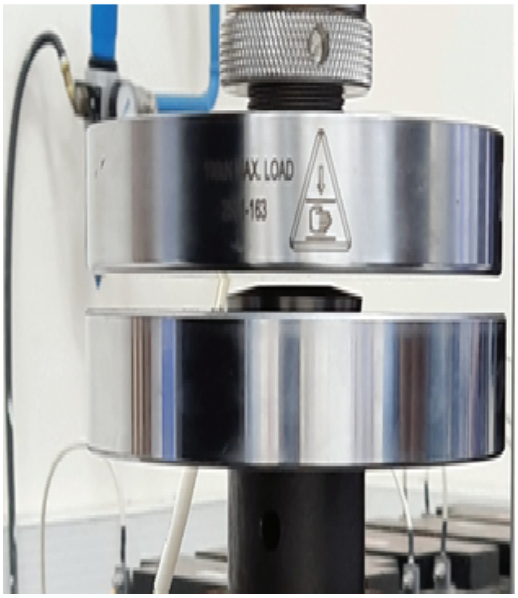

(b) Disc spring on UTM before loading

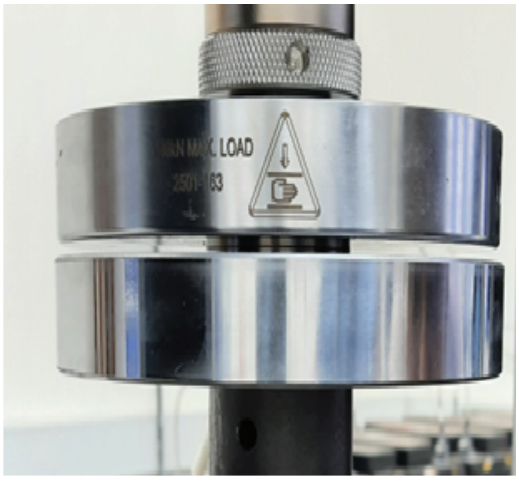

(c) Disc spring on UTM after loading

Figure 3. Different views of experiment on NTBS

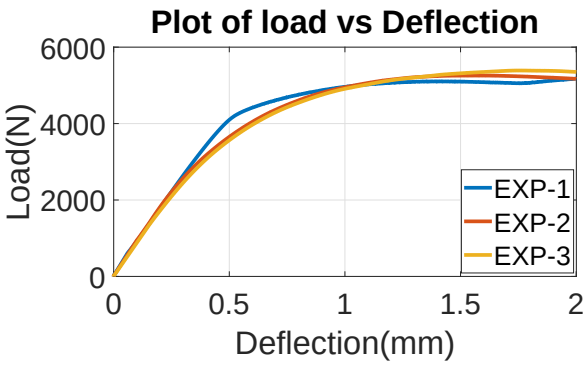


Figure 4. Load versus deflection plot for fabricated NTBS, a=25 mm, b=12.5 mm, E=195 Gpa

an axisymmetric four-node quadrilateral element (CAX4R), with a discretization number of four across the thickness. An axial enforced displacement is applied to the top edge of the spring, and the reaction force is computed at each converged iteration. The NTBS is free to slide along the outer diameter in the horizontal plane. The NTBS analyzed in this study is presumed to be composed of a homogeneous, isotropic, and elastic material, characterized by Young's modulus $E = 195$ GPa and a Poisson's ratio $\nu = 0.27$, Table 1. Geometric non-linearity is incorporated into the simulation and all contacts are assumed to be frictionless.

Fig. 6a shows a typical result obtained for a deflection of 2 mm using FEA and Table 1 data. The maximum elastic stress is 3877 MPa at the top of the inner radius of the spring which is much larger than the yield stress of SS304 material. Due to the high shear force, there is significant distortion and yielding in the section. It may be noted that the flat region observed in the load versus displacement is due to plastic deformation. To account for this plastic deformation, we resort to elastic-plastic FEA using a yield stress versus plastic strain database (25). The FEA for the same deflection, geometrical parameters and plastic deformation are shown in Fig. 6b. It can be seen that although the maximum stress drops to 613 MPa throughout the section, this value is still larger than the yield stress of SS304. Consequently, yielding becomes inevitable.

For benchmarking FEA, the data by Rosa et al. (8) is used. The results from the FEA are compared with Rosa et al. (8) theory. The maximum load error is at 6.1% at the '2h' deflection and 4.6% at the 'h' deflection (Fig. 5b). For the same configuration but with reduced thickness of the spring, FEA gives smaller stress Fig. 7 when compared to a thicker one (Fig. 5a).

Based on FEA, we can make the following main observations:

- Elastic FEA results are in-line with Rosa (8) with a 4.6% deviation at $h$ – see Fig. 5b.
- Stresses are maximum at the top of the inner radius and bottom of the outer radius and stresses are minimum at the center portion of the spring as shown in Fig. 6a.
- Stresses in the fabricated NTBS exceed the yield stress of SS304 (Fig. 6a).

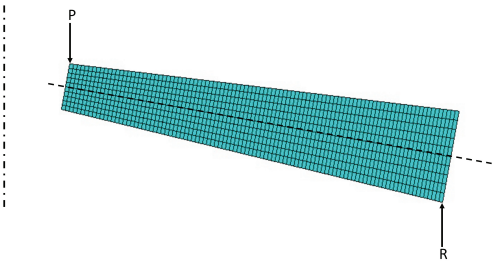


(a) Axis-symetric model for FEA analysis

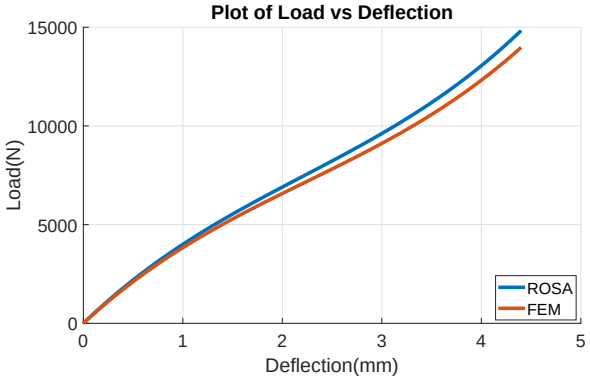


(b) Comparison of load deflection, FEA and Rosa's equation for $\tau = -0.325$, $a = 56$ mm, $b = 28.5$ mm, $h = 2.22$ mm, $E = 206$ GPa.

Figure 5. FE modeling and comparison with Rosa et al. (8)

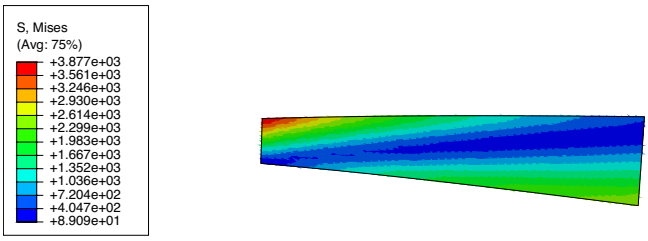


(a) von-Mises stress (MPa) in elastic deformed NTBS for $\tau = -0.33$, $a = 25$ mm, $b = 12.5$ mm, $h = 2.7$ mm.

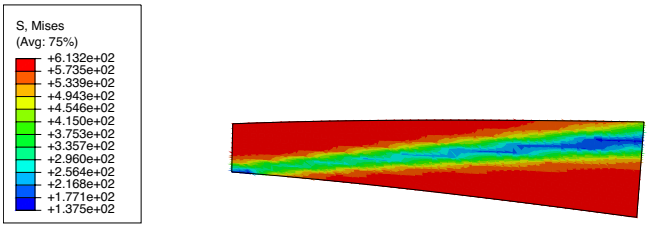


(b) von-Mises stress (MPa)in plastically deformed NTBS for $\tau = -0.33$, $a = 25$ mm, $b = 12.5$ mm, $h = 2.7$ mm.

Figure 6. FE simulation results for elastic and plastic deformation in NTBS

- Elastic-plastic FEA demonstrate a flat region similar to the experiment (see Fig. 8).

## Comparison of FEA and experiments

The elastic as well as elastic-plastic load deflection characteristics obtained from FEA are compared with

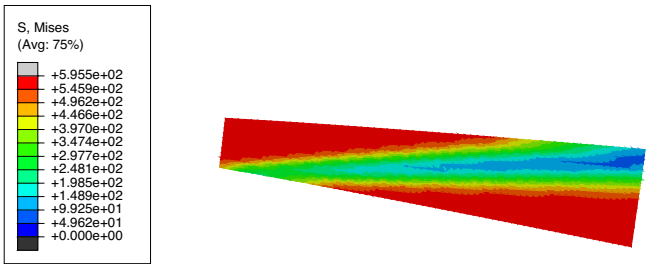


Figure 7. von-Mises stress (MPa) in elastic deformed NTBS $\tau = -0.33$, $a = 25$ mm, $b = 12.5$ mm, $h = 1.7$ mm, $t_c' = 1.2$ mm.

experimental results in Fig. 8. As expected the elastic load at 2 mm deflection of 11900 N is much larger than the experimental value due to plasticity. However, the elastic- plastic FEA matches well with the experiment at 0.75 mm deflection under a load of 4300 N. The difference between FEA and experimental data is less than 1%. After 0.75 mm deflection, the load decreases due to plastic flow.

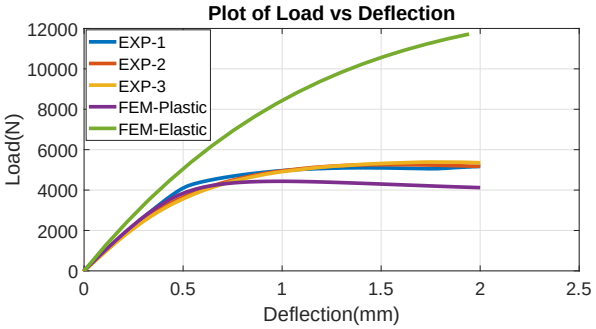


Figure 8. Comparison of FEA and Experiment result for $\tau = -0.33$, $a = 25$ mm, $b = 12.5$ mm, $h = 2.7$ mm.

In the next section, we present an improved elasticity model to predict TBS deflection including the null stiffness region.

## Theoretical Formulation

The TBS modeling is based on Timoshenko & Krieger (24) and Almen & Lazlo (5). The aim is to link the null stiffness region with Poisson's ratio. The improved TBS model is derived using the following assumptions:

1. Spring remains elastic
2. Uniform loading on the smaller radius
3. Frictionless contact
4. The cross-section of the spring rotates about a fixed point of the section throughout the deflection
5. The cross-section of the spring is undistorted during loading
6. Small initial angle of the spring
7. Small deflection
8. Radial stresses are neglected

Fig. 9 is the sectional view of NTBS with the outside thickness more than the inside thickness and the thickness linearly varying with the span length. Once

the uniform load $P$ is applied on the inner diameter of the NTBS, the whole spring starts to rotate about point 'O' and it deflects from a small angle $\beta$ to $\phi$. There exists a bending moment $M_1$ about the rotation point which leads to a change in curvature of the TBS. Associated with the change in curvature another bending moment $M_2$, is generated about the point 'O'. The two moments together resist the external moment generated by the applied external load (5).

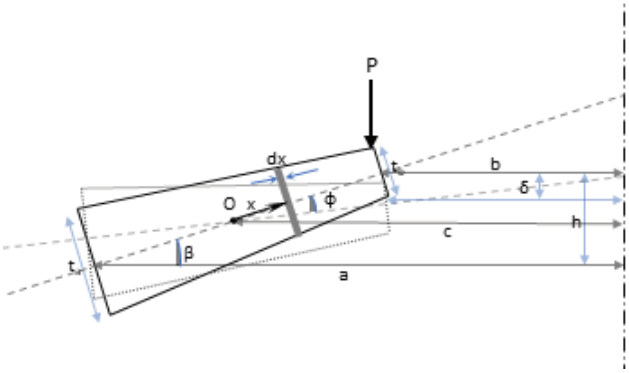


Figure 9. Section view of TBS

For a TBS with the thickness varying linearly, the thickness $T(x)$ at a distance $x$ from the point of rotation 'O' can be written as

$$T(x) = Ax + B \tag{1}$$

At the radii $r = b$, and $r = a$, we have

$$x = \frac{c-b}{\cos\beta} \text{ and } x = \frac{c-a}{\cos\beta}, \quad \text{respectively}$$

where $c$ is the distance as shown in Fig. 9. For small angle approximation $\cos\beta = 1$ and $\sin\beta = 0$ and we can write $x = c - b$ and $x = c - a$ at $r = b$ and $r = a$, respectively. Define $\tau$ as

$$\tau = \frac{t_b - t_a}{2t_{c'}} \tag{2}$$

where $t_{c'}$ is thickness at $r = \dfrac{a+b}{2}$. At $r = a, b$ and $\frac{a+b}{2}$ or $x = c - a, c - b$ and $\frac{1}{2}(2c - a - b)$, $T(x)$ is given by $t_a$, $t_b$ and $t_{c'}$, respectively. From equation (1), $A$ and $B$ can be written as

$$A = \frac{2\tau t_{c'}}{a-b}, \qquad B = t_{c'}\left(1 - \frac{2\tau c}{a-b} + \tau\left(\frac{a+b}{a-b}\right)\right) \tag{3}$$

and equation (1) can be written as,

$$T(x) = \frac{2\tau t_{c'}}{a-b}x + t_{c'}\left(1 - \frac{2\tau c}{a-b} + \tau\left(\frac{a+b}{a-b}\right)\right) \tag{4}$$

At a distance of $x$ from the rotation point, the tangential strain due to external load $P$ is given by (5)

$$\epsilon = \frac{x\phi\left(\beta - \frac{\phi}{2}\right)}{c-x} \tag{5}$$

and the tangential stress is given as

$$\sigma = E^*\epsilon = \frac{E^* x\phi\left(\beta - \frac{\phi}{2}\right)}{(1-\nu^2)(c-x)} \tag{6}$$

where, $E^* = \dfrac{E}{1-\upsilon^2}$, and $E$ is the Young's modulus of the spring and $\nu$ is the Poisson's ratio. It may be noted here that the Poisson's ratio is absent in reference (8).

For a strip $dx$ Fig. 9, the tangential stress will create a radial force given by

$$F = \sigma\, T(x)\, dx = \frac{E\left(\beta - \frac{\phi}{2}\right)}{(1-\nu^2)}\left(\int_{c-a}^{c-b}\frac{Ax^2}{c-x}dx + \int_{c-a}^{c-b}\frac{Bx}{c-x}dx\right) \tag{7}$$

and the radial moment due to radial force (5) is given by

$$M_1 = \frac{E\phi(\beta-\phi)\left(\beta - \frac{\phi}{2}\right)d\theta}{1-\nu^2}\int_{c-a}^{c-b}\frac{(Ax+B)x^2}{c-x}dx \tag{8}$$

The radial moment due to change in curvature (5) is given by

$$M_2 = \frac{E\phi d\theta}{12(1-\nu^2)}\int_{c-a}^{c-b}\frac{(Ax+B)^3}{c-x}dx \tag{9}$$

and the total internal moment on the disc is given by

$$M_{int} = M_1 + M_2 \tag{10}$$

The external moment due to load $P$, $M_{int}$ are related as

$$M_{\text{ext}} = M_{int} = \frac{P(a-b)d\theta}{2\pi} \tag{11}$$

For small angles $\beta = \dfrac{h}{a-b}$, $\phi = \dfrac{\delta}{a-b}$ where $h$ is the initial height of the spring and $\delta$ is the deflection due to the applied load $P$. Finally from equations (10) and (11),

$$P = \frac{2\pi E\delta}{(1-\nu^2)(a-b)^5}\left[(h-\delta)\left(h - \frac{\delta}{2}\right)t_{c'}U_1 + t_{c'}^3 U_2\right] \tag{12}$$

where,

$$U_1 = \frac{1}{3}\tau S_1 - \frac{1}{2}S_2 S_3$$

$$U_2 = \frac{1}{12}\left(6{S_3}^2 S_4\tau + \frac{4}{3}S_1\tau^3 - {S_3}^3 S_5 - 6S_3 S_2\tau^2\right)$$

$$S_1 = 6c^3\ln\left(\frac{a}{b}\right) - 18c^2(a-b) + 9c(a^2-b^2) - 2(a^3+b^3)$$

$$S_2 = 2c^2\ln\left(\frac{a}{b}\right) - 4ca + 4cb + a^2 - b^2$$

$$S_3 = 2c\tau - a\tau - b\tau - a + b$$

$$S_4 = b - a + c\ln\left(\frac{a}{b}\right)$$

$$S_5 = \ln\left(\frac{a}{b}\right)$$

The load equation (12) is the same as the one proposed by Rosa (8) if the Poisson's ratio $\nu$, is set to zero. It will be shown that the Poisson's ratio contributes more than 6.1% to the result with reference to Rosa et. al (8).

## Null load condition

As the name implies, the null load condition means $P = 0$ in the equation (12) and this gives

$$\frac{2\pi E\delta}{(1-\nu^2)(a-b)^5}\left[(h-\delta)\left(h-\frac{\delta}{2}\right)t_{c'}U_1 + t_{c'}^3 U_2\right] = 0 \tag{13}$$

The above cubic equation has three roots:

$$\delta_1 = 0, \delta_{2,3} = \frac{3}{2}h \pm \sqrt{9h^2 - 8\left(\frac{h^2U_1 + t_{c'}^2U_2}{U_1}\right)}$$

For real values of deflection $\delta$,

$$\frac{h}{t_{c'}} \geq 2\sqrt{2\left(\frac{U_2}{U_1}\right)} \tag{14}$$

When $\frac{h}{t_{c'}} = 2\sqrt{2}\sqrt{\frac{U_2}{U_1}}$ the spring will exhibit its snapping behaviour.

## Null stiffness condition

The region in the load-deformation curve where the slope of the curve is zero (or almost zero) is termed as the null stiffness region. This is obtained by setting $\frac{dP}{d\delta} = 0$. Using equation (12), the two roots are:

$$\delta_{4,5} = h \pm \sqrt{h^2 - \frac{2}{3}\left(\frac{h^2U_1 + t_{c'}^2U_2}{U_1}\right)}$$

For the null slope condition, the load at $\delta_4$ and $\delta_5$ will be nearly equal. For real values of $\delta$,

$$\frac{h}{t_{c'}} \geq \sqrt{2\left(\frac{U_2}{U_1}\right)} \tag{15}$$

A TBS that satisfies the condition in equation (15), will exhibit a null stiffness from $\delta_4$ to $\delta_5$. For the above range of deflection, the force will be constant. This type of spring is suitable for absorbing large impact energy without transferring the load to the next element of the system.

## Radius of rotation

The radius $c$ from rotation point O to the spring axis can be obtained using the condition that the summation of force at the neutral point, 'O', is equal to zero. Hence, for $\sum F = 0$, we get

$$\frac{E\phi\left(\beta - \frac{\phi}{2}\right)}{(1-\nu^2)}\left(\int_{c-a}^{c-b}\frac{Ax^2}{c-x}dx + \int_{c-a}^{c-b}\frac{Bx}{c-x}dx\right) = 0 \tag{16}$$

After evaluating the above integral and substituting for $A$ and $B$, we get the value of $c$ as

$$c = \frac{(a-b)^2}{(a-b)\ln\left(\frac{a}{b}\right) + \tau(a+b)\ln\left(\frac{a}{b}\right) - 2\tau(a-b)} \tag{17}$$

For the condition, $t_a = t_b$, or $\tau = 0$, we get

$$c = \frac{(a-b)}{\ln\left(\frac{a}{b}\right)}$$

which is a familiar result from Almen & Lazlo (5). From equation (17), a designer can fix the center of rotation $c$ of the spring, and then $\tau$ can be derived. This helps in designing instrumentation to find the rotation angle.

## Correction factor: theory of plates & shells

The NTBS stiffness predicted by Rosa et al. (8) is inconsistent with the elastic theory of plates when $h = 0$. In this section, we develop a correction factor to give a much better estimate of NTBS stiffness. This correction factor obviates the need for computationally intensive FEA for different geometries.

The theory of plates is well established (24). For a flat annular disk of inner radius $b$ and outer radius $a$ and uniform thickness $t$, The deflection $\delta$ is given by

$$\delta = \frac{Pr^2}{8\pi D}\left[\ln\left(\frac{r}{a}\right) - 1\right] - \frac{C_1 r^2}{4} - C_2\ln\left(\frac{r}{a}\right) + C_3 \tag{18}$$

At $r = b$ of an annular plate

$$C_1 = \frac{P}{4\pi D}\left[\left(\frac{1-\nu}{1+\nu}\right) - \frac{2b^2}{a^2-b^2}\ln\left(\frac{b}{a}\right)\right]$$

$$C_2 = -\frac{P}{4\pi D}\left[\left(\frac{1+\nu}{1-\nu}\right)\frac{a^2b^2}{a^2-b^2}\ln\left(\frac{b}{a}\right)\right]$$

$$C_3 = \frac{Pa^2}{8\pi D}\left[1 + \frac{1}{2}\left(\frac{1-\nu}{1+\nu}\right) - \frac{b^2}{a^2-b^2}\ln\left(\frac{b}{a}\right)\right]$$

$$D = \frac{Et^3}{12(1-\nu^2)} \tag{19}$$

For deflection at $r = b$ equation (18) can be written as

$$\delta = \frac{Pb^2}{8\pi D}\left[\ln\left(\frac{b}{a}\right) - 1\right] - \frac{C_1 b^2}{4} - C_2\ln\left(\frac{b}{a}\right) + C_3$$

From the above equation, the compliance $\frac{\delta}{P}$ denoted by $C_{FAP}$ can be determined as

$$C_{FAP} = \frac{b^2}{8\pi D}\left[\ln\left(\frac{b}{a}\right) - 1\right] - \frac{C_1 b^2}{4P} - \frac{C_2}{P}\ln\left(\frac{b}{a}\right) + \frac{C_3}{P} \tag{20}$$

Utilizing load equation (12), we get

$$P = \frac{2\pi E\delta}{(1-\nu^2)(a-b)^5}\left[(h-\delta)\left(h-\frac{\delta}{2}\right)t_{c'}U_1 + t_{c'}^3U_2\right]$$

and

$$\frac{P}{\delta} = \frac{2\pi E}{(1-\nu^2)(a-b)^5}\left[(h-\delta)\left(h-\frac{\delta}{2}\right)t_c' U_1 + t_c'^3 U_2\right] \tag{21}$$

The compliance of belleville spring, ($C_{FBS}$), can be written from equation (21) as

$$\begin{aligned} C_{FBS} &= \lim_{h\to 0,\delta\to 0}\left(\frac{\delta}{P}\right) \\ &= \frac{1.5(a-b)^5}{\pi D\left(18S_3^2S_4\tau + 4S_1\tau^3 - 3S_3^3S_5 - 18S_3S_2\tau^2\right)} \end{aligned} \tag{22}$$

By comparing equations (20) and (22), we define a correction factor $G$ as

$$G = 1 - \frac{24\,(a-b)^5\,(a^2-b^2)\,(1-\nu^2)}{MN} \tag{23}$$

where

$$\begin{aligned} M = 4\left(\ln\left(\frac{b}{a}\right)\right)^2 a^2b^2\,(\nu+1)^2 \\ -\left(a^2-b^2\right)\left(\nu^2+2\,\nu-3\right) \end{aligned}$$

and

$$N = \left(4S_1\tau^3 - 18\,S_2S_3\tau^2 - 3{S_3}^3S_5 + 18{S_3}^2S_4\tau\right)$$

The correction factor $G$ derived above is obtained from the compliance of a flat belleville spring and a flat annular plate.

For springs with $\tau < 0$ ( NTBS), the stiffness reduces in comparison to $\tau = 0$. At the same time the center of rotation of the section is at a larger distance from the axis of rotation. For the same deflection and projected area of the spring, the stiffness is less than the nominal stiffness of the UBS.

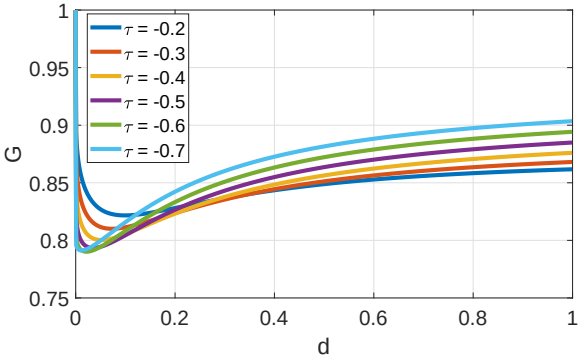


Figure 10. Variation of correction factor(G) with $d$ for different values of $\tau$

The correction factor depends upon $d = b/a$ and $\tau$ for a fixed Poisson's ratio. From Fig. 10, it can be seen that $G$ increases monotonically for $d \geq 0.2$.

To obtain a correct $P$ for a particular deflection, a designer has to fix $d$ and find $G$ from Fig. 10 and then use equation (24) given below

$$P = \frac{2\pi E\delta G}{(1-\nu^2)(a-b)^5}\left[(h-\delta)\left(h-\frac{\delta}{2}\right)t_{c'} U_1 + t_{c'}^3 U_2\right] \tag{24}$$

Figure 14 shows load versus deflection for four cases, namely equation (12) with Poisson's ratio, elastic and elastic - plastic FEA results from ABAQUS, and analytical model with correction factor. As mentioned earlier, Poisson's ratio increases the load compared to FEA by approximately 15%. This is for the geometry studied in this work with $G = 0.836$ (for $d = 0.5$, $\tau = -0.33$ and $t_c = 1.2$ mm). Figure 12 shows that the plot with the correction factor is very close to the FEA results with less than than 1% difference.

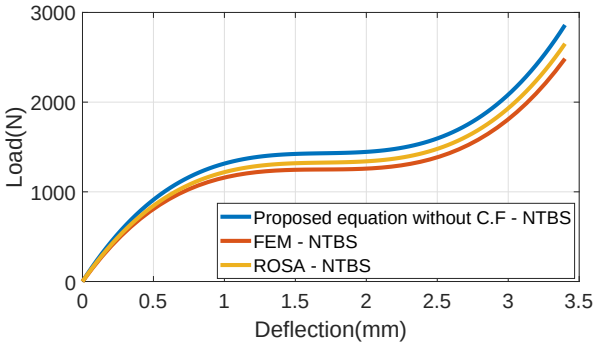


Figure 11. Comparison of load results of NTBS for $\tau = -0.33$, $a = 25$ mm, $b = 12.5$ mm, $h = 1.7$ mm.

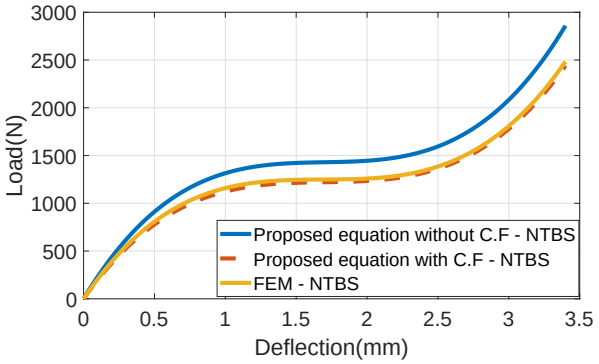


Figure 12. Proposed equation with correction factor converging with FEA result ($\tau = -0.33$, $a = 25$ mm, $b = 12.5$ mm, $h = 1.7$ mm).

We have performed extensive FEA on RTBS where $\tau > 0$. In this case, the thickness decreases as we move away from the axis of rotation of the spring with $t_b > t_a$. This implies that the stiffness, from the equation (12), is increasing in comparison to NTBS. At the same time the center of rotation of the section is nearer to the axis of rotation. Hence, the relative stiffness of the RTBS is greater than NTBS and UBS. A representative plot of load versus deflection for an RTBS ($\tau = 0.33$, $a = 25$ mm, $b = 12.5$ mm, $h = 1.7$ mm) is shown in Fig. 13. It can be seen that the match with FEA is reasonably good and the use of correction factor is not required.

Finally, we describe the FEA for the geometry of the belleville springs used in experiments. The deflection

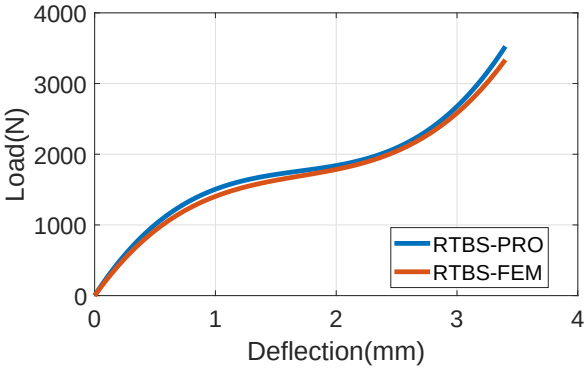


Figure 13. Comparison of load results of RTBS for proposed equation(PRO) and FEA $\tau = 0.33$, $a = 25$ mm, $b = 12.5$ mm, $h = 1.7$ mm.

limited to 2 mm due to experimental constraints is shown in Fig. 14. It can be observed that results with plasticity are quite different from those obtained from the elastic formulation, equation (12) and equation (24). It may be mentioned again that the FE simulation results with plasticity are close to the experimental results and the match is reasonable.

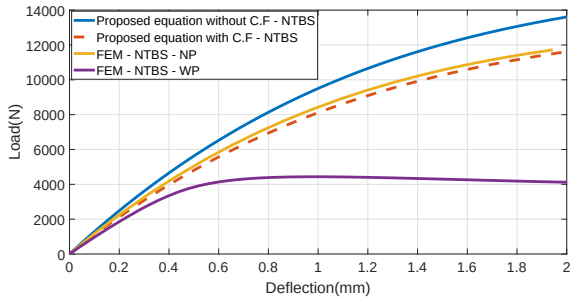


Figure 14. Comparison of theoretical and FEA (plasticity) results for $\tau = -0.33$, $a = 25$ mm, $b = 12.5$ mm, $h = 2.7$ mm.

In the next section, we look at the absorption of energy by a TBS and the use of the correction factor to predict the energy absorbed by a tapered belleville spring.

## Energy absorption

For a given $a$, $b$, and $t_c$, a TBS can be fabricated with any value of $\tau$ from -1 to 1, and the spring can take the shape of NTBS or RTBS. To optimize a TBS in terms of energy per unit volume, we start with the well-known expression for energy per unit volume

$$E = \int_0^h P d\delta \tag{25}$$

Using equations (24) and (25), $E$ can be written as

$$E = K\left(U_1 \int_0^h \delta(h-\delta)\left(h - \frac{\delta}{2}\right) d\delta + t_c^2 U_2 \int_0^h \delta d\delta\right) \tag{26}$$

where $K = \dfrac{2\pi E t_c}{(1-\nu^2)(a-b)^5}$

The energy of TBS at the deflection $\delta = h$ can be written as

$$E_{\text{TBS}} = K\left(\left(\frac{h^4}{8}\right)U_1 + \frac{h^2}{2}t_c^2 U_2\right) \tag{27}$$

The energy of uniform spring (UBS) can also be derived as below using load equation in reference (5) and is given by

$$E_{\text{UBS}} = K\left(\left(\frac{\delta^4}{8} - \frac{\delta^8 h}{2} + \frac{\delta^2 h^2}{2}\right)\frac{1}{M} + \frac{\delta^2}{2}t_c^2\frac{1}{N}\right) \tag{28}$$

The volume of a TBS is given by

$$V_R = \pi(t_a + t_b)\frac{(a-b)}{\cos\beta}\left(a - \frac{(t_a + 2t_b)}{3(a+b)}\frac{(a-b)}{\cos\beta}\right) \tag{29}$$

$$V_N = \pi(t_a + t_b)\frac{(a-b)}{\cos\beta}\left(b + \frac{(t_b + 2t_a)}{3(a+b)}\frac{(a-b)}{\cos\beta}\right) \tag{30}$$

where $V_R$ and $V_N$ are the volume of RTBS and NTBS, respectively.

The volume of UBS is given by

$$V = \frac{(a^2 - b^2)\pi t}{\cos\beta} \tag{31}$$

The energy density can be calculated by dividing the energy of the spring at a particular deflection by its volume. For a fixed $a$, $b$, $t_c$, it is found that RTBS stores more energy than NTBS and a UBS. The energy density of RTBS is almost 35% and 27% higher than the energy density of NTBS and UBS respectively for the selected $\tau$ range.

## Effect of correction factor on energy absorption

The energy equation (28) is modified as

$$E = \frac{2\pi E t_c G}{(1-\nu^2)(a-b)^5}\left(\left(\frac{h^4}{8}\right)U_1 + \frac{h^2}{2}t_c^2 U_2\right) \tag{32}$$

Thus the energy can be increased by selecting the higher value of the $\tau$ from Fig. 10.

## Design considerations for a TBS

In this section, the design parameters of a TBS are explored from an impact energy absorption point of view. For impact energy absorption purposes, we would like the TBS to satisfy the null stiffness condition equation (14). Hence, we study the null stiffness condition for varying values of $\tau$ for TBS, as shown in Fig. 15. It is observed that for $\tau = 0$ (UBS), $\dfrac{h}{t_{c'}} = \sqrt{2}$, which is the same as the null stiffness condition obtained by Almen & Lazlo (5). For the same positive and negative value of $\tau$, $\dfrac{h}{t}$ curves are a pair of curves symmetric about a horizontal line and converging as $d$ tends to 1. From practical considerations, $a$ and $h$ can be fixed for a given application and we can find an appropriate $d$ between 0.2 and 0.6 as after $d = 0.6$

the plots converge and the ratio $h/t$ has no effect. For $\frac{h}{t_{c'}} = \sqrt{2}$, representing the null stiffness condition, $t_{c'}$ is obtained for a given value of $h$. Finally, $t_a$ and $t_b$ are obtained for the calculated $t_{c'}$.

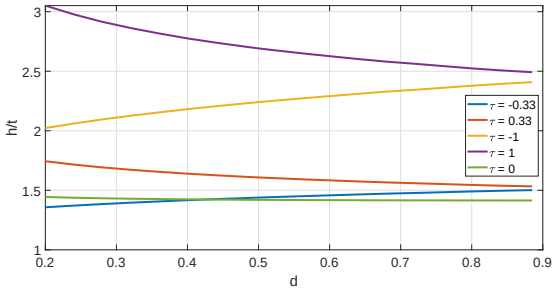


Figure 15. Variation of height to thickness ratio for null stiffness condition with respect to $d$

Another consideration from an experimentation and instrumentation point of view is as follows: from equation (17), for the values of $\tau$ ranging from $-1$ to 1 and $a = 25$ mm and $b = 12.5$ mm, it can be observed that $c$ varies almost linearly with $\tau$. For $\tau = -1$, $c =$ 20.37 mm, for $\tau = 1$, $c$ =16.18 mm, and at $\tau = 0$, $c$ is obtained as 18.03 mm and this value is identical to that given in Almen & Lazlo (5). For our case of $\tau = -0.33$, $c = 18.75$ mm. It may be noted that for a fixed value of $a$ and $b$, and $-1 < \tau < 1$, the value of $c$ can be obtained. If it is desired that $c$ is exactly $(a + b)/2$, the corresponding $\tau$ can be obtained from the plot. The above helps to identify the point of rotation in a fabricated TBS and for instrumentation on a TBS for strain measurement.

It is understood from equation (32) that energy can be increased by choosing an optimum pair of $G$ and $d$. The correction factor $G$ presented in this work needs to be used for estimating the actual energy storage capacity in a belleville spring.

## Belleville spring under cyclic loading

Multiple experiments were conducted on the fabricated TBS. In one experiment, cyclic loading and unloading was done in steps as 0 – 0.5 mm – 0, 0 – 0.75 mm – 0, 0 – 1.0 mm – 0, 0 – 1.5 mm – 0, 0 – 1.75 mm – 0, 0 – 2.0 mm – 0 and 0 – 2.5 mm – 0 (see Fig. 16). It is interesting to note in this figure that the second loading cycle reaching 4000 N gives a signal of yielding at a slightly higher displacement than in Fig. 8 dealing with monotonic loading. It was found that the loading and unloading caused hysteresis which could be explained by plastic yielding confirmed by elastic-plastic FEA. Almost half of the energy was lost due to plastic deformation as seen in the experiments (see Fig. 16). When all the cyclic plots were connected, it was observed that a single spring of 50 mm diameter can absorb around 6.5 J of energy. For a given load, multiple springs in series can be stacked to absorb more energy. The flat region occurs well before the peak load and deflection predicted by elastic theory. The elastic-plastic response also leads to hysteresis in cyclic loading. Numerical predictions are consistent with experimental results obtained for an SS304 spring material (see Table 1). Further research on hysteresis and residual stress induced by plasticity is needed for better understanding.

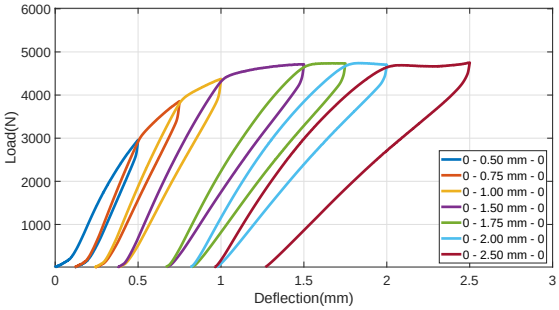


Figure 16. Cyclic loading experiment results on fabricated TBS

## Discussion

The compact nature of beleville spring and its ability to produce null stiffness zone in stiffness plot motivates us to design the TBS for impact absorption. The SS304 - NTBS for $\tau = -0.33$ was designed for small size (Table 1) and experiments were done on them. In experiments, NTBS yielded. This is due to the large thickness and the spring angle of the fabricated spring which makes the spring behave more like a beam resulting in large shear. Hence, the proper combination of the geometric parameters of NTBS is necessary for an optimum spring design. The comparison of experimental and simulation results is based on similar geometrical dimensions, similar material and mechanical properties, and similar boundary conditions. The experimental load deflection plot is validated with the simulation result. For the same projected area, the FEA of NTBS and RTBS confirms that the energy density of RTBS is more than NTBS. It can also be concluded that RTBS is suitable for higher load applications and NTBS is suitable for higher impact energy absorption.

## Conclusion

This work deals with experiments, modeling and analysis of small sized belleville springs. The geometric non-linearity in a belleville spring and its ability to produce a null stiffness zone in a stiffness plot motivates one to design and use a belleville spring for impact absorption. In this work, small sized SS304 NTBS were fabricated and experiments were done. Experimentally it was found that a flat region in the load-deflection plot was due to yielding and not demonstrating null stiffness due to non linear elasticity. Elastic FEA showed a significantly higher load than elastic-plastic FEA which matched well with experimental results for small deflection.

In order to supplement FEA results for different geometries, a theoretical development including the effect of Poisson's ratio is presented. The results

obtained are compared with FEA for TBS in the elastic range. It is observed that the analytical loads are higher by 15% for NTBS and within 4% for RTBS, as compared to FEA. A correction factor for NTBS is introduced based on the classical theory of plates. For typical dimensions of the spring, the differences between FEA and the analytical model after applying the correction factor is reduced to less than 1%. The FEA also shows that for the same projected area of the spring, RTBS can store up to 35% more energy than NTBS and 27% more energy than UBS. The main findings of this paper are a) Poisson's ratio makes a difference in the TBS load equation, b) Analytical loads are 15% higher than the FE simulation load, c) Correction factor reduces the differences in load from 15% to 1% for NTBS , and d) RTBS can absorbs 35% more energy than NTBS and 27% more than UBS. This paper also presents an approach for the design of TBS from a null stiffness point of view.

In this work, we show that previous theoretical formulations result for TBS were not in line with FEA. A correction factor introduced in this work improves the theoretical formulation to give nearer results as compared to those obtained from FEA. In future, the friction effect on TBS and load versus deflection for a stacked TBS will be studied.

Further experiments are planned with belleville springs made of high-strength alloys, in stacked series and parallel arrangements, for achieving higher energy storage and impact absorption. As observed in the experiments, friction and plasticity are additional complexities and these dissipative mechanisms induce residual stress which requires further theoretical and numerical investigations.

Table 2. Nomenclatures used in the formulation

| Symbol | Description |
|---|---|
| T(x) | Thickness at any point |
| A,B | Thickness constant |
| $\tau$ | Shape factor |
| $a$ | Outer radius |
| $b$ | Inner radius |
| $d$ | Ratio of $b/a$ |
| $G$ | Correction factor |
| $t_{c'}$ | Thickness at $(a+b)/2$ |
| $\beta$ | Initial angle of disc spring |
| $\phi$ | Change in angle |
| $h$ | Initial height of the disc |
| $t_a$ | Thickness at the radius $a$ |
| $t_b$ | Thickness at the radius $b$ |
| $\delta$ | deflection of the disc |
| $O$ | center of rotation |
| $c$ | Radius at point O |
| P | Load applied |
| $\epsilon$ | Tangential strain |
| $\sigma$ | Radial stress |
| E | Young modulus |
| $\nu$ | Poisson's ratio |
| $M_1$, $M_2$ | Moments |
| $d\theta$ | Angle of the small strip on the disc |
| M, N | Correction factor variable |
| $C_{FBS}$ | Compliance of flat belleville spring |
| $C_{FAP}$ | Compliance of flat annular plate |
| SS | Stainless steel |
| BS | Belleville Spring |
| UBS | Uniform Belleville Spring |
| TBS | Taper Belleville Spring |
| NTBS | Normal Taper Belleville Spring |
| RTBS | Reverse Taper Belleville Spring |

## Acknowledgment

The author is grateful to Dr. Rajeev Chaturvedi and Dr. Nazeer Ahmed for providing useful inputs during this work.

## Nomenclature

## References

[1] Chidambarathanu G, Nair V and Stanis S. Structural analysis of belleville spring used in automatic shift transmission multi-plate wet clutch for off-highway application. SAE Technical Paper 2020-28-0491, 2020 2020; 2(28). DOI:10.4271/2020-28-0491.

[2] Mrazek M, Skovajsa M and Sedlacek F. Design of composite disc spring for automotive suspension with using numerical simulation. Manufacturing Technology 2022; 21(6): 829–835. DOI:10.21062/mft.2021.100. URL https://doi.org/10.21062/mft.2021.100.

[3] Schonrr A. Handbook for disc springs 2010; .

[4] Hui AM, Yan M, Zhang L et al. Shock characteristics of the opposed disc springs (ODS) shock isolator with pretightening under boundary friction condition. Shock and Vibration 2021; 2021: 1–21. DOI:10.1155/2021/5510200. URL https://doi.org/10.1155/2021/5510200.

[5] Almen J and Lazlo A. The uniform–section disk spring. Trans ASME 1936; 2(13): 68–73.

[6] Kobelev V. Durability of Springs. Springer International Publishing, 2018. DOI:10.1007/978-3-319-58478-2. URL https://doi.org/10.1007/978-3-319-58478-2.

[7] Du X, Liao C, Gan B et al. Analytical modeling and experimental verification for linearly gradient thickness disk springs. Thin-Walled Structures 2021; 167: 108153. DOI:10.1016/j.tws.2021.108153. URL https://doi.org/10.1016/j.tws.2021.108153.

[8] Rosa GL, Messina M and Risitano A. Stiffness of variable thickness belleville springs. Journal of Mechanical Design 1998; 123(2): 294–299. DOI:10.1115/1.1357162. URL https://doi.org/10.1115/1.1357162.

[9] Saini PK, Kumar P and Tandon P. Design and analysis of radially tapered disc springs with parabolically varying thickness. Proceedings of the Institution of Mechanical Engineers, Part C: Journal of Mechanical Engineering Science 2007; 221(2): 151–158. DOI:10.1243/0954406jmes114. URL https://doi.org/10.1243/

0954406jmes114.

[10] Fawazi N, Lee JY and Oh JE. A load–displacement prediction for a bended slotted disc using the energy method. Proceedings of the Institution of Mechanical Engineers, Part C: Journal of Mechanical Engineering Science 2011; 226(8): 2126–2137. DOI: 10.1177/0954406211430046. URL https://doi.org/10.1177/0954406211430046.

[11] Pedersen NL and Pedersen P. Stiffness and design for strength of trapezoidal belleville springs. The Journal of Strain Analysis for Engineering Design 2011; 46(8): 825–836. DOI:10.1177/0309324711414337. URL https://doi.org/10.1177/0309324711414337.

[12] Dubey H. Stress and deflection analysis of belleville spring. IOSR Journal of Mechanical and Civil Engineering 2012; 2(5): 01–06. DOI:10.9790/1684-0250106. URL https://doi.org/10.9790/1684-0250106.

[13] Ramhormozian S, Clifton GC, MacRae GA et al. Stiffness-based approach for belleville springs use in friction sliding structural connections. Journal of Constructional Steel Research 2017; 138: 340–356. DOI: 10.1016/j.jcsr.2017.07.009. URL https://doi.org/10.1016/j.jcsr.2017.07.009.

[14] Venkatesh DL and Zhou H. Designing belleville spring washers. International Journal of Engineering Research and 2018; V7(12). DOI:10.17577/ijertv7is120044. URL https://doi.org/10.17577/ijertv7is120044.

[15] Zhu D, Ding F, Liu H et al. Mechanical property analysis of disc spring. Journal of the Brazilian Society of Mechanical Sciences and Engineering 2018; 40(4). DOI:10.1007/s40430-018-1152-2. URL https://doi.org/10.1007/s40430-018-1152-2.

[16] Chaturvedi R, Trikha M and Simha K. Theoretical and numerical analysis of stepped disk spring. Thin-Walled Structures 2019; 136: 162–174. DOI:10.1016/j.tws.2018.12.003. URL https://doi.org/10.1016/j.tws.2018.12.003.

[17] Leininger DS, Geilen MB, Klein M et al. A new method for the calculation of characteristics of disc springs with trapezoidal cross-sections and rounded edges. Materials 2022; 15(5): 1954. DOI:10.3390/ma15051954. URL https://doi.org/10.3390/ma15051954.

[18] Ferrari G. A new calculation method for belleville disc springs with contact flats and reduced thickness. International Journal of Manufacturing, Materials, and Mechanical Engineering 2013; 3(2): 63–73. DOI:10.4018/ijmmme.2013040105. URL https://doi.org/10.4018/ijmmme.2013040105.

[19] Paredes M and Daidié A. Optimal catalogue selection and custom design of belleville spring arrangements. International Journal on Interactive Design and Manufacturing (IJIDeM) 2009; 4(1): 51–59. DOI: 10.1007/s12008-009-0086-4. URL https://doi.org/10.1007/s12008-009-0086-4.

[20] Maharjan D, Shah MS, Abugharara A et al. Calculating frictional losses in belleville springs by linear interpolation. In Progress in Canadian Mechanical Engineering. Volume 3. University of Prince Edward Island. Robertson Library. DOI:10.32393/csme.2020.1287. URL https://doi.org/10.32393/csme.2020.1287.

[21] Xiao SJ, Xu LH and Li ZX. Design and experimental verification of disc spring devices in self-centering reinforced concrete shear walls. Structural Control and Health Monitoring 2020; 27(7). DOI:10.1002/stc.2549. URL https://doi.org/10.1002/stc.2549.

[22] Mastricola NP, Dreyer JT and Singh R. Analytical and experimental characterization of nonlinear coned disk springs with focus on edge friction contribution to force-deflection hysteresis. Mechanical Systems and Signal Processing 2017; 91: 215–232. DOI:10.1016/j.ymssp.2017.01.009. URL https://doi.org/10.1016/j.ymssp.2017.01.009.

[23] Dassault Systéms. Abaqus 2020; .

[24] Timoshenko S. Theory of plates and shells 1959; 2.

[25] Rack HJ and Knorovsky GA. Assessment of stress-strain data suitable for finite-element elastic–plastic analysis of shipping containers ; DOI:10.2172/6513543. URL https://www.osti.gov/biblio/6513543.